ROYAL SOCIETY
OF CHEMISTRY

PAPER

Check for updates

Selective laser processing of particle accelerator beam screen surfaces for electron cloud mitigation†

Elena Bez,[ab] Ana Karen Reascos Portilla,[a] Valentine Petit, [a]
Konstantinos Paraschou,[a] Lotta Mether, [a] Kristóf Brunner,[a] Patrick Krkotić, [a]
Yasemin Askar,[a] Sergio Calatroni, [a] Mauro Taborelli[a] and Marcel Himmerlich [*a]

Laser-induced surface roughening is a technique that facilitates the reduction of secondary electron emission (SEE) from materials, which is crucial for mitigating electron cloud (EC) formation in particle accelerators, that operate with positively charged species, such as the large hadron collider (LHC). This study focuses on the development of a selective laser surface treatment of the inner copper surface of beam screens (BS) within superconducting (SC) magnets. Several technical challenges linked to laser processing exist including the reduction of treatment time and the control of ablation depth. Based on the found correlations between laser treatment parameters and materials properties, and considering all technical constraints for execution of such a process in SC magnets, a tailored laser processing strategy is developed, which includes creation of a rough Cu surface with trenches of 15–20 μm depth and an initial secondary electron yield maximum of 1.4–1.5, only in the most relevant regions of the BS. Resulting material properties are characterized such as the surface resistance and related beam impedance, as well as the SEE at both room temperature and cryogenic conditions. The efficiency to mitigate EC formation and thus improve beam quality is demonstrated *via* EC simulations and electron-induced conditioning experiments. This study also explores under which circumstances the risk of particulate detachment from the surface, which could lead to critical beam interaction, can be minimized.

1 Introduction

In view of the high luminosity upgrade of the large hadron collider (LHC)[1,2] at the European Organization for Nuclear Research (CERN), the effect of electron cloud (EC) formation in the beam vacuum system during operation is predicted to be significantly enhanced.[3,4] This has consequences on the heat load that has to be extracted by the cryogenic cooling system as well as on the quality of the proton beam. The extent of the local electron density is directly linked to the properties of the inner surface of the beam screens (BSs), that are directly facing the proton beam. In the LHC the BS consists of a 75 μm thick oxygen-free electronic grade (OFE) Cu layer laminated onto stainless steel. The relevant material parameter is the secondary electron yield (SEY), which for Cu depends strongly on the oxidation state and the existence and nature of other impurities at the surface.[5,6] Several surface

treatment technologies have been developed in the past years to functionalize the inner surfaces of the BSs that can either be applied *in situ* in the installations in the LHC tunnel during a shut-down, or while a superconducting (SC) magnet is in overhaul outside the LHC tunnel, or during the production of new BSs before insertion into the SC magnet. The baseline technology for future upgrades is to coat the Cu surface with a functional layer of graphite-like amorphous carbon (a-C) with Ti interlayer using plasma-based sputtering from targets. This is an efficient way of reducing the maximum of the SEY in dependence of electron impact energy δ_{max} to values as low as 0.9,[7–9] which is far below the electron multipacting threshold in many regions of the CERN accelerator complex.[10] The technology has been already successfully applied to a series of magnets of the super proton synchrotron (SPS)[11] as well as to one standalone magnet in the LHC[12] during its long shutdown (LS) 2, and is going to be applied in most SC magnets in the straight sections around the ALICE[13] and LHCb[14] detectors during LS 3 for the high-luminosity LHC (HL-LHC) operation to start afterwards. In addition, all newly installed magnet assemblies around the CMS[15] and ATLAS[16] detectors are going to be equipped with a-C coated BSs in LS 3.

a CERN, European Organization for Nuclear Research, 1211 Geneva 23, Switzerland. E-mail: marcel.himmerlich@cern.ch
b University of Leipzig, Linnéstraße 5, 04103 Leipzig, Germany

© 2025 The Author(s). Published by the Royal Society of Chemistry

RSC Appl. Interfaces, 2025, **2**, 521–533 | 521

An alternative approach for SEY reduction is to selectively modify the Cu surface *via* scanning a focused ultrashort-pulsed laser beam across the Cu surface, which thereby roughens. The method has been demonstrated to be effective on a laboratory scale[17] and has already demonstrated electron cloud mitigation in a test stand of the SPS.[18] The resulting surface micro- and nanostructures can be tailored by varying the processing parameters such as the average laser power or the scanning speed[19–22] with direct influence on the SEY.[23] Laser modification has been selected as a potential surface treatment to be applied inside the Q5 standalone magnets of the straight sections next to CMS and ATLAS during LS 3. It is anticipated that the electron could build-up in these magnets will result in a deterioration of the proton beam quality, potentially leading to beam losses or instabilities.[2,24–26] While the cryogenic complexes in the arcs of the LHC, including the main dipole and quadrupole magnets, are operated at 1.9 K, the cryogenic reservoir of the standalone magnets in the straight sections of the LHC are held at 4.2 K. To compensate the consequences of the higher base temperature and to ensure the cryopumping of hydrogen molecules[27] in the beam vacuum, the Q5 magnets are equipped with so-called cryosorbers made of carbon fiber fabric. This carbon based tissue has a very large effective surface and is attached to the CuBe pumping slot shields fixed on the cooling lines outside the BS (see Fig. 1). The presence of this functional element would result in outgassing and incorporation of impurities in the a-C films during *in situ* plasma coating of the BS. While the a-C coating technology therefore cannot be applied with full efficiency in those magnets, laser roughening has the advantage of being able to treat only selected regions of the BS surface and to omit technological problems. This study describes a possible solution based on laser surface processing of the BS inner surfaces that could be applied to SC magnets equipped with cryosorbers to mitigate EC formation.

2 Technical considerations for surface processing in the LHC vacuum system at ambient conditions

A series of conditions must be fulfilled for the processing of LHC beam screens in SC magnets up to 10 m in length and the resulting surfaces are required to meet certain specifications to assure safe operation of the UHV vacuum system, both with and without particle beams. The laser processing induces material ablation. The resulting crater depth should not exceed 25 μm to prevent a significant increase in the surface impedance. The surface impedance significantly impacts both the beam stability and the beam-induced resistive wall heating. Previous studies[29,30] have shown that the surface resistance of laser-treated Cu not only increases with greater groove depth but also depends on the orientation of the grooves relative to the induced surface current. This finding is crucial for defining the optimal laser
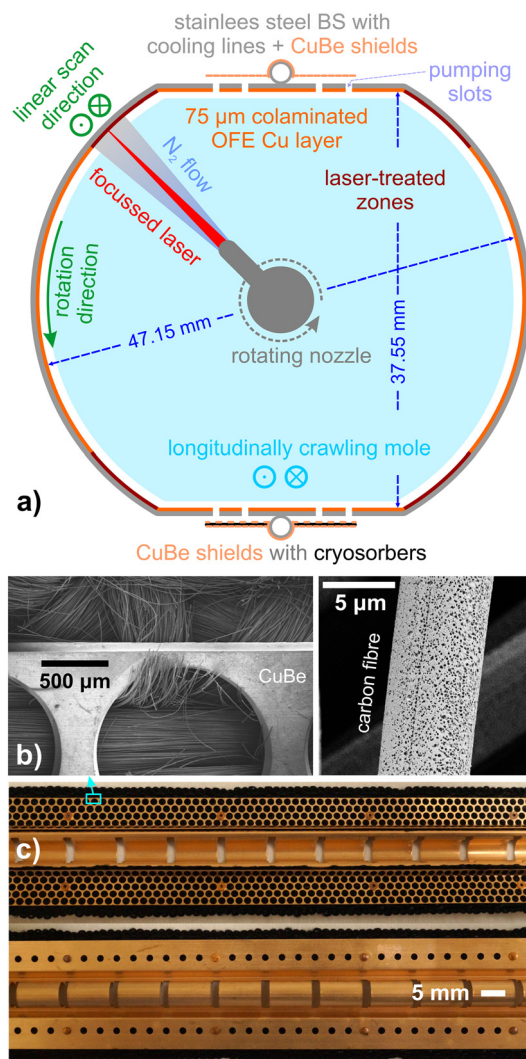

Fig. 1 a) Cross-section of the 50L⁺ beam screen type that is installed in the LHC Q5 quadrupole magnet including an illustration of the basic principle of local selective laser scanning *via* a longitudinally moving inchworm robot and a rotating nozzle.[28] The laser spot is scanned longitudinally in parallel lines in the regions next to the 4 corners (each covering 20° of the full circumference). The treated zones are highlighted in brown, while the untreated Cu regions are orange. b) Scanning electron micrographs of the CuBe pumping slot shields with cryosorbers (left), which consist of carbon fibers woven to a fabric, and of the surface of a single fiber (right). This element is installed on the bottom of the BS in the horizontal configuration. c) Photographs of inner and outer side of the CuBe pumping slot shields with cryosorbers (black).

processing pattern, *i.e.* the formed trenches shall ideally align with the direction of circulating beam-induced image currents in the beam screen surface.

Furthermore, the number of loosely attached particulates remaining on the BS surface after the laser treatment should be minimal and their diameter should not exceed 60 μm.[31] Otherwise, in case of their detachment followed by a possible collision with the proton beam, the created radiation could lead to high signals in the surrounding beam loss monitors and thus trigger a beam dump to prevent severe damage of the SC magnets. Such events would not be compatible with

accelerator operation. When laser processing is performed in a confined geometry, the ablated particulates tend to accumulate at the bottom of the chamber, even if an extraction system is used. Therefore, a good strategy is to minimize the ablated volume *via* limiting the treatment to the zones of high electron cloud density, which are dependent on the magnetic field symmetry,[32,33] and combine this with a subsequent process to remove these particulates.

The SEY maximum of laser-treated copper can be decreased to values as low as 0.7 when applying relatively high photon flux.[17,23] As the surface and electron emission properties depend on the applied laser fluence,[23] this processing parameter can be used to optimize the surface transformation in order to match the needs in terms of limiting the number of attached and distributed loose particulates, the ablation volume and thus the change in surface resistance. For effective EC mitigation, the SEY maximum should be below the formation threshold, which depends on the type of magnet and its beam aperture.[33] In the LHC, for most constellations a $\delta_{max} \leq 1.1$ is sufficient, while values below unity would suppress any multiplication tendency. In addition, a metallic surface with adsorbates will reduce its SEY when being exposed to a flux of electrons. This process is referred to as electron conditioning. Copper surfaces that had been laser-roughened at fairly low laser fluence exhibit typically an SEY maximum above unity. It was recently demonstrated that a sample with an initial SEY maximum of 1.5 after processing still has the capability to reach values of $\delta_{max} \leq 1$ during conditioning,[23] *i.e.* a condition in which no EC can build up anymore.

Fig. 1a) shows a schematic of the cross-section of the BS in the Q5 magnets (type 50 L$^+$), which has a truncated circular shape with inner diameter of 47.15 mm. The truncated planar regions have elongated holes which act as pumping slots to allow residual gas molecules to escape the beam pipe and to be cryosorbed at the outer cold bore surface. The slots are covered by shields made of copper–beryllium (CuBe) from which some are equipped with the cryosorber fabric. Fig. 1b) and c) include scanning electron micrographs and photographs of these functional elements. An inchworm robot is crawling inside the BS and allows to scan the focused laser beam across the inner BS surface while gaseous N_2 is blown into the interaction zone to suppress oxidation.[28] It is self-evident that a direct scanning of the laser spot across the pumping slots should be avoided to not damage the cryosorber fibers and contaminate the BS surface. Consequently, the laser treatment is not ideal for dipole field magnets equipped with cryosorbers, in which the reduction of the SEY in the flat BS regions would be essential for electron mitigation.[33,34] For quadrupole magnet fields, the electron–BS interaction regions are very narrow bands located on the circular part near the corners. A selective laser treatment in these zones, *i.e.* in four regions each covering 20° of the full circumference (see brown zones in Fig. 1a)) appear, based on simple geometric considerations, to be sufficient for a mitigation of the electron multiplication in

this case (called 4 × 20° pattern from now on). Two experimental advantages are eminent for this scenario: i) treating only 22% of the whole circumference reduces the processing time and the amount of ablated material/particulates very significantly, and ii) processing in the curved regions ensures a constant distance between the surface and the optics and no adjustment of the focal point of the laser is necessary. The used robot is capable of selectively scanning the focused laser spot in lines with a spacing of 50 μm that are parallel with respect to the BS axis.

As a consequence of the aspects discussed above and especially considering the transformation processes at Cu surfaces during electron conditioning,[6,23,35] our study focuses on a relatively mild laser surface processing technique that enables an initial SEY maximum of 1.4–1.5 of the Cu surface after treatment with the capability of further SEY reduction induced by electron conditioning to reach $\delta_{max} \leq 1$. This approach will also limit the ablation and trench depth to 15–20 μm. We address the requirements for a selective treatment of beam screens in patterns aligned with the magnetic field and electron cloud distribution in LHC quadrupole magnets and examine the topography, composition, SEY, electron conditioning behavior at room temperature and cryogenic conditions, and particulate release of the laser treated surface. By including electron cloud and beam interaction simulations as well as beam screen surface resistance measurements, we demonstrate that the approach of a selective treatment pattern is effective to mitigate EC formation and thus beam quality deterioration in quadrupole SC magnets and that no significant change of the surface impedance results from the laser-induced transformation process.

3 Simulation and experimental methods

3.1 Simulation of electron cloud and beam interaction

The formation of the electron cloud in the Q5 standalone magnets is simulated with the PyECLOUD[36] software. In PyECLOUD, a particle-in-cell approach is used to track the motion of the electrons under the influence of i) the static magnetic field produced by the magnet, ii) the dynamic electromagnetic fields induced by the passage of the particle beams, and iii) the forces induced by the electron cloud's own space-charge. The fields of the particle beams and the EC are calculated by solving the Poisson equation with a finite-difference method while the Boris algorithm is used to advance the electrons.[34] Since the particle beams that typically produce electron clouds are highly relativistic, an ultra-relativistic approximation is used and the particle beams are assumed to travel at the speed of light. This approximation greatly simplifies the problem such that a two-dimensional simulation of a transverse cross section of the beam screen is sufficient to describe the electron cloud in the entirety of the magnet.[37]

In addition, a secondary emission model is required to simulate the interaction of electrons impinging on the beam screen's surface.[38] The model is based on both laboratory-based material characterization of secondary electron emission and beam measurements[33] of the LHC beam screen, and is frequently used to predict the heat load deposited by the EC during LHC operations. To model laser-treated surfaces, the measurement of the secondary electron yield's dependence on the primary electron energy, which is presented further below, is used assuming a fully conditioned surface.

The effect of the electron cloud on the particle beam is associated with the proximity of beam particles to large electron densities.[39–41] The impact on the beam quality will therefore be minimized by ensuring the profile of the EC does not show large densities close to the beam's location.

3.2 Laser surface treatment and sample preparation

To process the inner surface of a beam screen segment for surface resistance measurements a dedicated laser treatment setup was used, which consists of an infrared ultrashort pulse laser source (Trumpf TruMicro 2030), an optical system designed to couple the laser pulses into a hollow-core photonic crystal fiber, and an inchworm robot that travels inside the BS to perform the treatment. The configuration of the setup is analogous to that described in ref. 28, with the exception that in the present setup an infrared laser (1030 nm, 1 ps, 500 kHz) is used and the hollow-core photonic crystal has a 7-cell 3-ring kagome structure with a core diameter of 60 μm. A plano-convex lens with a focal length of 84 mm was used to focus the Gaussian laser beam onto the curved regions of the beam screen's inner surface to a spot size of 49 μm. Nitrogen was blown into the reaction zone of the laser to minimize oxidation during the process. Prior to the laser treatment of the 40 cm long beam screen segment as well as smaller test samples, the specimen were wet-chemically degreased with a commercial detergent (DP 17.40 SUP from NGL Cleaning Technology SA, Switzerland) and subsequently rinsed with de-ionized water. The inner part of a 40 cm long beam screen segment (type 50 A) with a diameter of 46.75 mm was irradiated using a scanning speed of 20 mm s^{-1}, a line distance of 50 μm, and an average laser power of 6.5 W applying the selective treatment at the four corners of the BS according to the 4 × 20° pattern. The accumulated fluence under these conditions was 530 J cm^{-2}. For the required surface analyses, a second beam screen was processed using identical conditions and witness samples were subsequently cut from it. In addition, oxygen-free (OFE) copper samples (12 × 15 mm^2) were used for particulate detachment and electron conditioning tests. They were inserted into squared holes in the curved beam screen regions so that their inner surfaces are flush. These samples were processed at different scanning speeds and average laser powers to vary the accumulated laser fluence and to create surfaces with different SEY values. The tests were performed using samples from several BS dimensions (46.75 mm to 80 mm inner diameter). Prior to any subsequent characterization, the test samples were exposed to a stream of compressed gaseous N$_2$ to blow loose particulates off the surface.

3.3 Material characterization

Standard room-temperature SEY measurements were performed in an ultrahigh vacuum (UHV) system using the sample-bias method. The experimental details are described in ref. 23 and 42. The laser-treated surface was further characterized and electron-conditioned at room temperature and at 15 K in a second UHV system with a base pressure of 6 × 10^{-10} mbar. For electron conditioning the samples were irradiated with 250 eV electrons supplied by a scanned electron gun (EQ 22/35) on a square of size of 10 × 10 mm^2. After defined electron doses, the SEY was measured and the surface chemical composition was characterized *via* X-ray photoelectron spectroscopy (XPS). In this setup a collector-based method is employed for the SEY measurement, with a voltage of +53.3 V applied to the collector and −19.1 V to the sample. The XPS measurements are performed using a non-monochromated MgKα X-ray source (*hv* = 1253.6) and a Phoibos 150 hemispherical electron analyzer equipped with 9 channeltrons. The system is described in more detail elsewhere.[43,44] The surface topography was characterized using a field emission gun scanning electron microscope (FEG-SEM) Sigma 500 (ZEISS) with InLens secondary electron and Everhart–Thornley secondary electron (SE2) at an accelerating voltage of 10 kV. In addition, a Veeco NT3300 white light interferometer (WLI) was used to measure surface profiles.

Redeposited particulates from the ablation process can potentially detach when a force is acting on them. During beam operation of the LHC, such species may fall into the proton beam and trigger beam losses. For this reason, it is important to quantify the number of detaching particulates. A maximum force density of 30 Nm m^{-3} (ref. 45) acts on the beam screen surface during a quench, in which the magnet surrounding the beam screen looses its superconductivity state within a few hundred milliseconds. As the proton beam is extracted from the accelerator in the event of a magnet quench, any further falling particulates do not affect the quality of the beam. Therefore, a lower force density of 3 N mm^{-3}, representing 10% of the maximum force density, was selected for this study to estimate the possible maximum number of particulates released during operation of the LHC, and potentially inducing beam losses or dumps.

The experimental setup is shown in Fig. 2. The laser-treated samples were placed in one side of a sample holder and a carbon sticker attached to the other half is facing it after assembly without direct contact. The sample holder was installed in a centrifuge (Beckman Coulter Optima
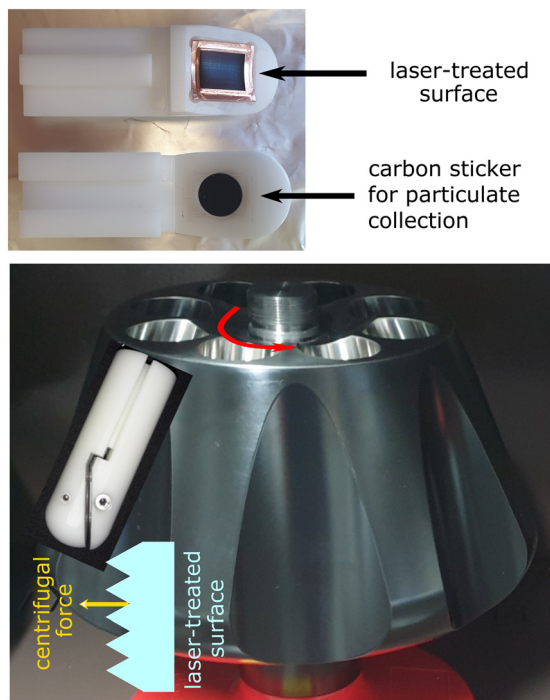
Fig. 2 Experimental setup for particulate detachment tests. Top row: Photograph of disassembled sample holder. Bottom row: Rotor with installed sample holder and schematic of centrifugal force acting on the laser-treated surface.

L-100 XP ultra-centrifuge with Beckman Coulter 70 Ti rotor) with the laser-treated surface facing outward and a counterweight was placed on the opposite side to balance the rotor to an accuracy of 0.0001 g. The number of particulates collected on the sticker as well as their equivalent circular diameter (ECD) were determined by automated particulate analysis (APA) using a FEG-SEM Sigma (ZEISS) at 20 kV with SE2 and back scattered electron (AsB) detectors in combination with a 50 mm^2 X-Max energy dispersive X-ray spectroscopy (EDS) detector and the related data analysis procedures in the AzTEC software from Oxford Instruments.

A comprehensive theory to predict the surface resistance of laser treated rough surfaces has not yet been established. Therefore, an experimental setup based on the shielded pair method[46,47] was used to measure the surface resistance of the LHC beam screen to quantify the impact of the chosen 4 × 20° laser treatment pattern. This technique utilizes the beam screen under study as a resonating body closed at each end with copper-plated end caps. Additionally, two hollow, copper-plated stainless steel rods are inserted into the center of the beam screen, serving two purposes: i) to obtain resonance frequencies within the LHC's relevant beam spectrum (*i.e.*, less than 2 GHz), and ii) to excite two closely spaced resonances separately, allowing for the discrimination of the rods' losses and thereby independent quantification of the beam screen's losses. The shielded pair device can assess surface resistance within the frequency range between 400

and 1200 MHz and at temperatures ranging from 4.2 K to room temperature.

4 Results and discussion

4.1 Electron cloud simulation of selective treatment

The calculations take into account as input for the simulations the flattened primary electron energy dependence of the SEY for laser-roughened copper surfaces, which differs from that of planar surfaces[48] and varies with changing laser fluence during processing.[20,23] During the formation of the EC, the electrons are trapped around the lines of the magnetic field. For this reason, they tend to form characteristic cross-shaped density profiles in quadrupole magnetic fields, like the one illustrated in the top left of Fig. 3 that shows the result of a PyECLOUD buildup simulation. As a result, a particle beam that is centered in the magnet can suffer from the electromagnetic forces that are induced by the strong local electron densities in its vicinity. This simulation was performed using HL-LHC beam operation parameters[2] that maximize the number of electrons in the cloud, which include a bunch intensity of 1.8×10^{11} protons per bunch with bunches spaced at 25 ns and a surface with a maximum secondary electron yield of $\delta_{max} = 1.5$ of the whole BS surface. It is important to note that the model used for the untreated surfaces is conservative in order to take into account any possible present or future degradation of the untreated beam screen surface in operation after electron-conditioning – variations exist for the SEY maximum that can be reached depending on the surface oxidation state of the flat Cu surface[6] after conditioning. One has to keep in mind that during LHC operation, the conditioning state will depend on the local electron doses that the different BS zones are exposed to, which will not lead to a homogeneous SEY distribution and the likelihood that the SEY of regions without electron impact could be higher than 1.5. Nonetheless, the model electron cloud calculations can demonstrate the tendencies of a local laser treatment with laser-roughened zones that condition to a SEY maximum of 1.0 upon electron impact.

The top right and bottom left graphs in Fig. 3 show the simulation of the density profile with a selective treatment of ±1° and ±6° around the 45° diagonals. The corners of the beam screen (highlighted in orange) are modeled with $\delta_{max} = 1.0$ to consider the effects of the laser-treatment and conditioning during operation, while δ_{max} remained at 1.5 for the other regions. By treating the corners of the beam screen, the electron density is depleted inside the area around the beam, which is indicated by the black dashed lines (extending up to five times the r.m.s. size of the beam). Although the total number of electrons can be in the same order of magnitude as without the surface treatment, the impact to the beam quality is mitigated by them being located far from the center. Finally, the bottom right of Fig. 3 shows the simulation considering the 4 × 20° pattern, where

© 2025 The Author(s). Published by the Royal Society of Chemistry

RSC Appl. Interfaces, 2025, **2**, 521–533 | **525**
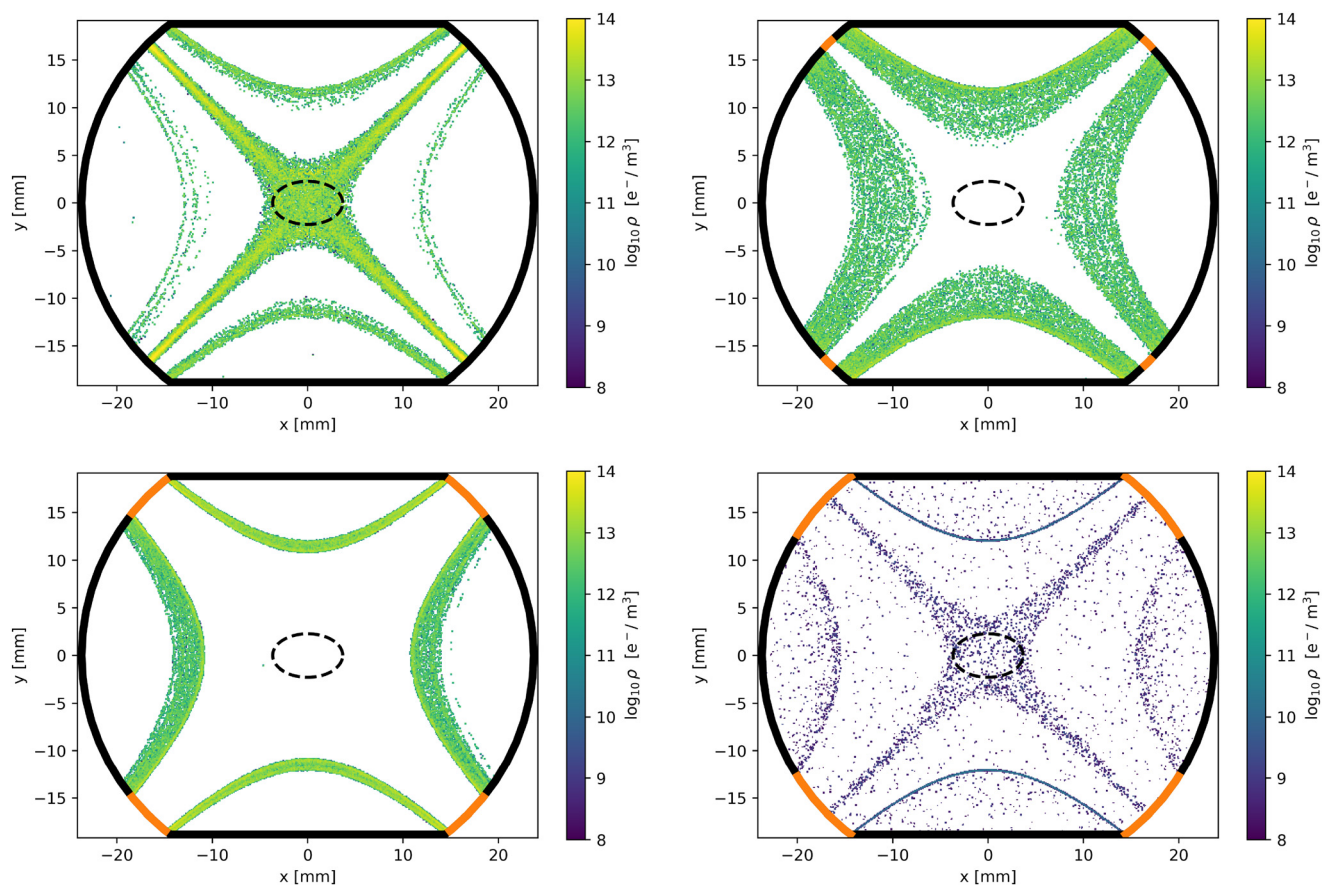
Fig. 3 Electron cloud density profile simulations with effective models of untreated (maximum SEY of 1.5) and laser-treated (maximum SEY of 1) surfaces for a 7 TeV proton beam of 1.8×10^{11} protons per bunch with 25 ns bunch spacing. Top left: Untreated surface. Top right: Treated surface covering ±1° around the 45° diagonals (highlighted in orange). Bottom left: Treated surface covering ±6° around the 45° diagonals. Bottom right: Treated surface following the 4 × 20° pattern.

the electron distribution does not exhibit multipacting, and therefore the electron density is several orders of magnitude lower.

By increasing the extent of the treated surface, the electrons tend to get trapped further and further away from the center of the magnetic field inside the BS until multipacting stops. A coverage as small as ±1° around the 45° diagonals appears enough to deplete the area around the beam from strong local electron densities. However, it is advantageous to increase this coverage in order to guard against possible misalignment or rotation of the beam screen with respect to the magnetic axis of the SC magnet. Furthermore, certain margins and inaccuracies in the local laser processing of very long beam screens with the experimental setup need to be considered as well. The 4 × 20° selection is a good compromise. The results of these simulations give clear guidelines for the local laser processing and prove the selective modification around the regions of high electron impact during beam operation to be sufficient to mitigate the multipacting and EC build-up in quadrupole magnetic fields. They also indicate that the treated regions could be minimized to a very narrow angular range when a maximum SEY of 1 is obtained.

4.2 Laser-treated beam screen segment – surface properties

Fig. 4 (top) displays a photograph of a beam screen processed with the selective 4 × 20° pattern, including four dark stripes at the corners of the BS that were laser-treated, while the untreated copper surface remained mirror-like. The stripe on the right side of the BS inner surface represents the sawtooth profile imprinted in the beam screens external side, which is present to reduce the forward-reflection of the synchrotron radiation generated during beam operation.[27,49,50] Fig. 4 includes at its bottom a line scan and 2D topography map of the laser-treated surface. As the ps-laser pulse irradiation leads to significant local material ablation, micro-trenches are formed, that are aligned with the scanning direction of the laser spot, which was chosen to be parallel to the BS axis. The average depth of the cross-sectional profile amounted to 15 ± 2 μm. In contrast, the depth of the region in the opposite corner of the BS was slightly greater (19 ± 1 μm). This variation of the ablation depth in different azimuths of the BS is attributed to a slight under-/over-focus, which occurs since the rotating mirror within the robot is not always perfectly centered within the BS as some space is required for the clamping and movement of the inchworm
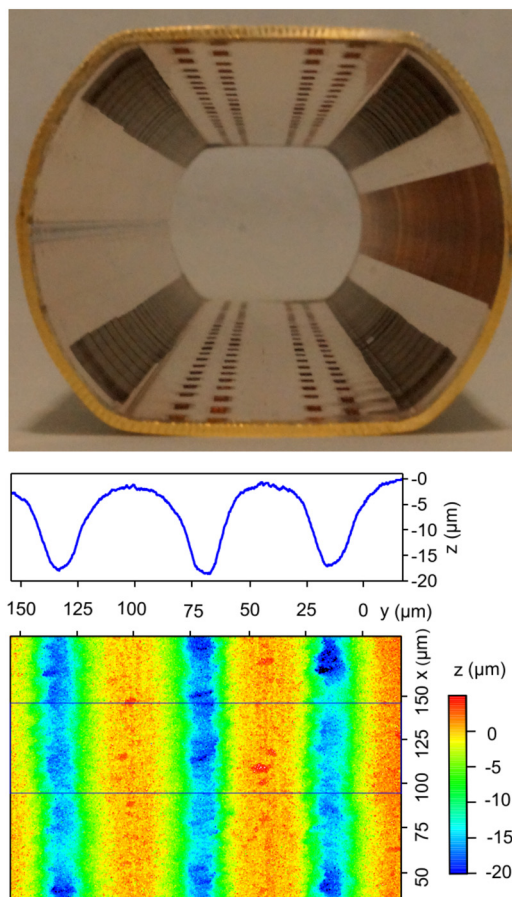
Fig. 4 Top: Cross-sectional photograph of the 40 cm long beam screen after finalization of the selective laser treatment. Four regions of 20° azimuthal width each at the corners were laser-processed and appear dark, while untreated regions remain bright. The band in the center right is the sawtooth profile for reduction of synchrotron light reflection (see text for more information). Bottom: Line profile and 2D map of the laser-structured surface topography.

robot. Therefore, slight distance differences of up to 0.5 mm can occur for the different azimuth angles, which is roughly half of the Rayleigh length of the beam. As a result, the laser spot at incidence is slightly wider and the light intensity reduced, which leads to a lower ablation rate. This aspect was already discussed in our earlier study[28] and for the used accumulated fluence of 530 J cm^{-2}, comparable ablation depths were obtained in laser irradiation experiments on flat surfaces.[23]

Fig. 5 compares scanning electron micrographs of these samples: the one with deeper trenches is on the left side. Both samples have a similar surface topography with the micrometer-scale deep trenches being formed in the regions of highest local laser intensity, in which ablation processes are initiated as discussed above. Adjacent to this laser spot center, in the tails of the Gaussian beam profile, the light intensity is lower so that no significant ablation results. Therefore, ridges remain in between the trenches and the actual aspect ratio and topography depends on the processing parameters.[19] In these regions, the transformation
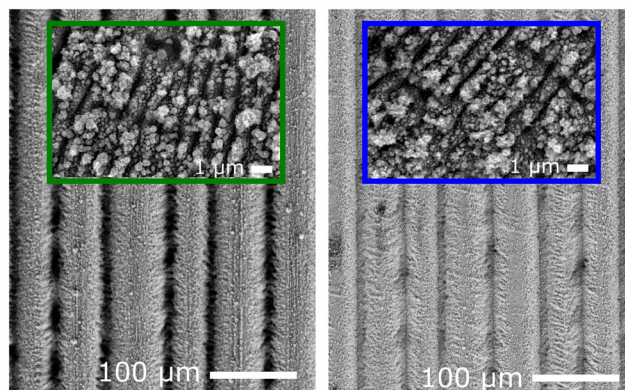

Fig. 5 Scanning electron micrographs of the laser-processed surfaces extracted from two opposite corners of the beam screen. The inserts visualize the nanofeatures on top of the ridges of the formed surface topography.

process induced the formation of laser induced periodic surface structures (LIPSS),[51] which typically occurs at lower photon fluxes.[52] These micro-features are decorated by nanoparticulates which were redeposited from the plasma plume formed during ablation.

The primary electron energy dependence (50 to 1800 eV) of the secondary electron yield of the two samples at room temperature is shown in Fig. 6. The maximum SEY of the sample with larger ablation depth is 1.28 at a primary electron energy of 1100, while that of the sample with shallower trenches is 1.52 at the same primary electron energy. The standard deviation of both SEY experiments based on measurements of several spots across the treated samples was negligibly small (0.01), which indicates a homogeneous surface modification on macroscopic scale. The difference in the SEY is in accordance with a change in local photon
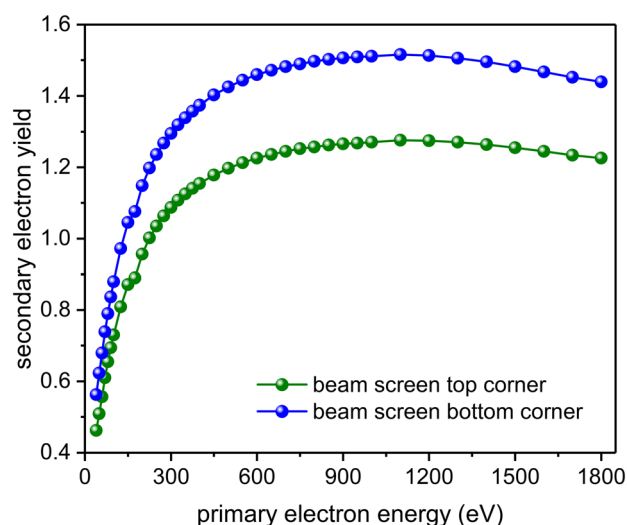

Fig. 6 Room temperature secondary electron yield of two samples extracted from opposite corners of the selectively-treated beam screen (average of three measured spots). The corresponding SEM images are plotted in Fig. 5.

© 2025 The Author(s). Published by the Royal Society of Chemistry

RSC Appl. Interfaces, 2025, **2**, 521–533 | **527**

density due to over-/under-focus. Slight variations in light intensity can have nonlinear effects on the resulting SEY, especially for processing with infrared light.[23] Compared to a smooth unprocessed and detergent-cleaned copper surface,[5] the SEY maximum of the laser-treated surface was reduced due to the roughening effect from values >2 before modification to the targeted initial value of ≤ 1.5 after treatment, which has been demonstrated to be suitable to suppress EC activity after a first phase of electron-irradiation at room temperature,[23] equivalent to electron-induced effects during beam scrubbing in the accelerator environment. However, a characterization of the conditioning effects at cryogenic conditions has not been performed up to now.

4.3 Laser-treated surfaces – characterization of particulate detachment

The laser process results in the redeposition of nanoparticulates that are initially expelled from the surface during ablation and then fall back onto the substrate. During the time of flight and the post-ablation equilibration, these clusters can reach the Cu substrate surface still warm and establish a bonding with it. Nonetheless, the fragile structure[53] does not in all circumstances form a very stable bonding to the substrate and there is a potential risk that some particulates could detach from the surface if an external force is present. To assess this risk, laser-treated surfaces with SEY maxima in the range between 0.9 and 1.8 were subjected to centrifugal forces. The global number of detached particulates per surface area of a selection of samples is shown in Fig. 7. Almost no particulates were released from the surfaces exhibiting an initial SEY maximum $\delta_{max} \geq 1.1$ after processing (without conditioning).
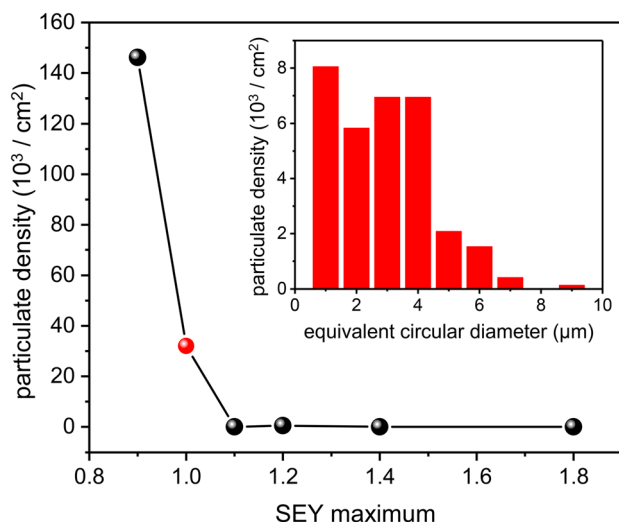

Fig. 7 Summary of centrifugation tests applying a force density of 3 N mm^{-3}. The graph shows the number of detached particles per unit area as a function of the maximum SEY of the laser treated surface. The size-distribution of the equivalent diameter of collected particles for the case of the surface with SEY maximum of 1.0 (red data point) is shown in the inset.

Thus, the aforementioned beam screen treatment is within this category and the particulates are not expected to fall at a force density of 3 N mm^{-3}. We note that the selective treatment prevents particulates from falling directly into the proton beam during LHC operation by gravitational forces due to the exclusion of the top part of the beam screen. The higher the laser fluence during surface processing, the lower is the SEY of the surface, the deeper is the microstructure, and the more particulates cover the surface.[20,23] Therefore, the number of collected particulates increased to 150 000 per cm^2 for surfaces with $\delta_{max} \leq 1$. The inset of Fig. 7 illustrates the distribution of particulates as a function of their diameter for one selected sample with $\delta_{max} = 1.0$. The diameter of all detached particulates was smaller than 10 μm, with an average value of 2 μm. This is of particular significance, given that the proton beam interaction with particulates with a diameter greater than 10 μm may induce beam losses and larger particulates (≥ 60 μm diameter) can cause severe damage to the accelerator due to generated radiation.[31] This damage is typically prevented by a beam dump, whereby the beam is extracted from the machine. In conclusion, for the optimized surface laser processing conditions, a surface structure can be obtained that does not possess a strong risk of particulate release during operation.

4.4 Laser-treated surfaces – surface modifications induced by electron conditioning at room temperature and at 15 K

As the laser treatment is intended to mitigate electron clouds in the vacuum chambers of superconducting magnet complexes, the surface conditioning effect, *i.e.* the change of the SEY and composition upon electron irradiation, was evaluated at both room temperature and 15 K using two identical laser-structured Cu test samples which have comparable surface properties as those of the processed beam screen. Prior to conditioning, the SEY maximum of the two surfaces amounted to 1.4 at room temperature. At 15 K, the δ_{max} increased to 1.5, which is a result of adsorption of residual gas molecules even if the system base pressure is in the 10^{-10} mbar range. The top graph in Fig. 8 shows a semi-logarithmic plot of the SEY maximum in dependence of electron dose to which the surfaces were expose to. At room temperature and at 15 K a linear trend can be seen on this scale. In both tests the surfaces reached $\delta_{max} = 1$ at a dose around 0.01 C mm^{-2}. Electron multiplication is completely suppressed for $\delta \leq 1$. However, electron clouds in most regions of the LHC do not form if the SEY of the beam screen surface is below 1.1,[10] while the heat load threshold depends on the type of SC magnet (dipole or quadruple magnetic field) and the proton bunch population.[33] Doses of 0.001 C mm^{-2} are sufficient to reach this scenario for the laser processing conditions under discussion in this manuscript. No surface charging was observed during the measurement, in contrast to previously reported results on a cryogenic conditioning of a laser-treated surface.[18] This is linked to the different surface composition in our case since strong surface

oxidation during laser treatment was prevented *via* utilization of a N_2 inert gas flow.[28] The bottom graph of Fig. 8 includes the primary electron energy dependence of the SEY for selected conditioning steps. The shape of the SEY curve, which differs from that of an untreated Cu sample significantly,[5,28] remains stable, while the absolute values reduce proportionally.

The SEY maximum of the surface generally decreases due to chemical reactions that are induced during the electron irradiation process.[5] XPS measurements were conducted after each conditioning step to characterize the chemical transformation of the surface. The variation of the O 1s and Cu $2p_{3/2}$ XPS spectra as well as the carbon content at the surfaces (in at%) in dependence of electron dose during conditioning at RT and at 15 K are shown in Fig. 9. At the start of the experiment, the topmost layer of both surfaces

comprised a mixture of Cu_2O and $Cu(OH)_2$, as evidenced by the double peak positions of the Cu $2p_{3/2}$ state at binding energies (BE) of 932.8 eV and 934.5 eV in combination with the Auger transition at a kinetic energy (KE) of 916.7 eV (the corresponding spectra can be found in figure 5.18 of ref. 54). The shape of the Cu $2p_{3/2}$ satellite feature between 938 and 948 eV also indicates the presence of $Cu(OH)_2$.[55] During the RT conditioning, the $Cu(OH)_2$ spectral features vanished, the O 1s line shifted to a BE of 530.4 eV, while the Cu LMM state remained at 916.7 eV KE. These observations are consistent with the expected transformation of $Cu(OH)_2$ to Cu_2O (ref. 5 and 56) and partial desorption of species during room-temperature conditioning.

The electron irradiation at 15 K resulted in a different surface stoichiometry. The related changes can be understood in terms of electron-induced desorption and adsorbate transformation reactions at the Cu surface. Most notably the change in the satellite structure of the Cu $2p_{3/2}$ state is not as significant and rather a partial change to the spectral fingerprint of CuO (ref. 55) with enhancement of the second satellite feature at 941.0 eV and retention of a shoulder around 935 eV occurs. In accordance, the maximum
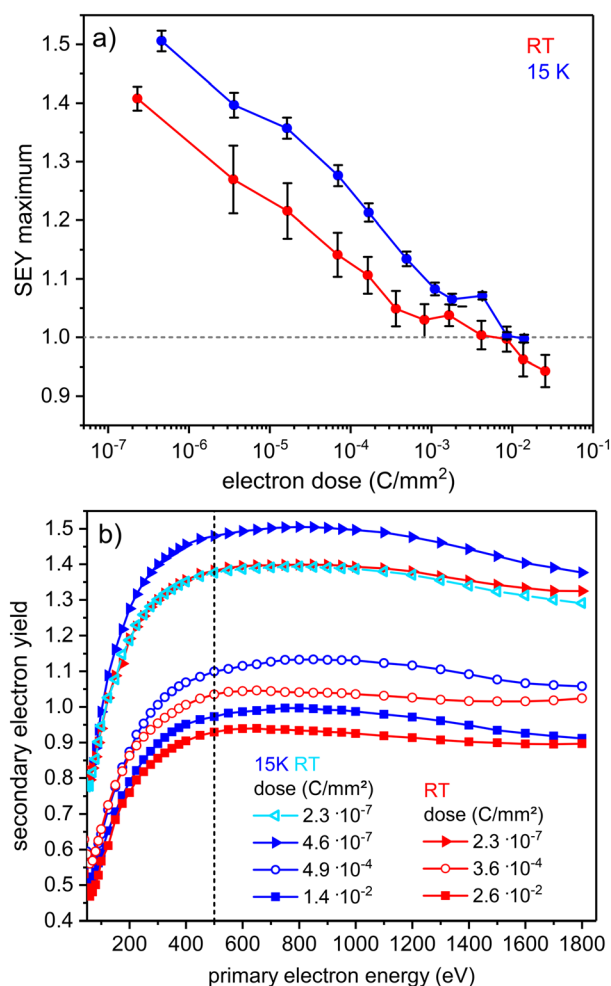

Fig. 8 Electron-irradiation experiments at room temperature and 15 K of two identical laser-treated OFE copper insert samples. a) SEY maximum in dependence of electron dose during exposure. The horizontal dashed line indicates the desired SEY value, at which electron clouds are guaranteed to be suppressed in the LHC since no multipacting can occur. b) SEY curves as a function of primary electron energy for selected electron doses. The energy range up to 500 eV is of particular interest (indicated by the vertical dashed line), as the number of electrons in the LHC is highest in this range.
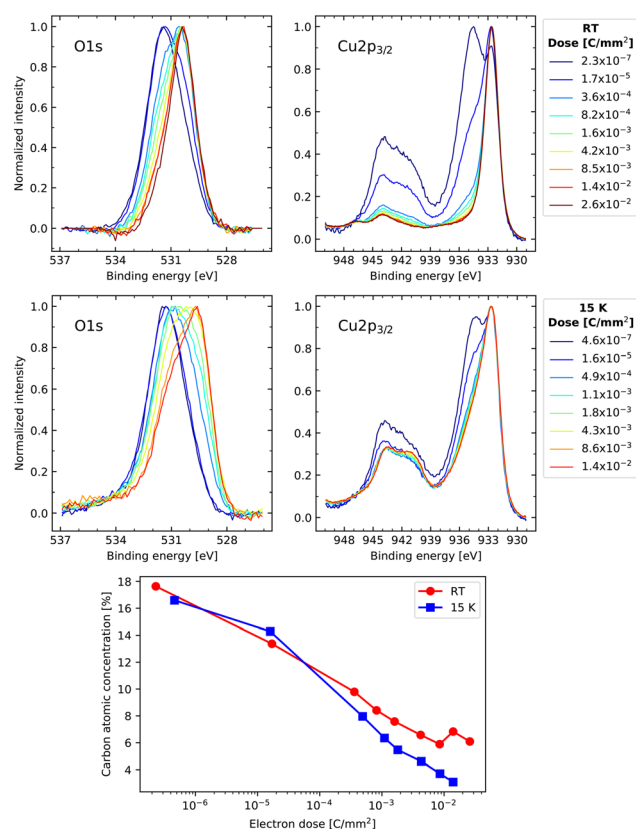

Fig. 9 Chemical surface analysis by XPS during the room temperature and cryogenic electron-conditioning of laser-treated Cu surfaces with initial δ_{max} = 1.4. Top and middle: Background-subtracted O 1s and Cu $2p_{3/2}$ core level spectra after exposure to increasing electron doses at room temperature and 15 K, respectively. Bottom: Reduction of the surface carbon content during the electron-induced transformation processes.

© 2025 The Author(s). Published by the Royal Society of Chemistry

RSC Appl. Interfaces, 2025, **2**, 521–533 | **529**

of the O 1s spectrum shifted to a lower BE of 529.6 eV and that of the Cu LMM transition to a KE of 917.8 eV. Consequently, $Cu(OH)_2$ was partially converted into CuO at this low temperature. This phenomenon of different oxidation behavior of the Cu surface at cryogenic temperature was also found on Cu components extracted from the LHC as well as during electron irradiation in model experiments at 15 K.[6,57] The partial formation of CuO leads to an insignificantly higher SEY after conditioning compared to a Cu_2O surface. In addition, for both electron-induced conditioning experiments at either room temperature or 15 K, the surface carbon content gradually decreased for increasing electron doses (see bottom of Fig. 9, the corresponding spectra can be found in figure 5.18 of ref. 54) as a result of partial desorption of hydrocarbon species and partial chemical transformation of the carbon adsorbates.[5] Nonetheless, the involved surface reactions during electron impact are complex and the detailed analysis of the influencing factors and their consequences on the SEY are a subject of an ongoing study to be reported in the near future.

It is noteworthy that the found differences in surface stoichiometry transformation as a function of temperature during electron conditioning, especially the chemical trends at cryogenic conditions, do for these laser-treated surfaces not have such a significant consequence on the final SEY and potential heat load or beam deterioration in particle accelerator operation as for flat Cu (ref. 6) – an SEY maximum of unity is reached at $\sim 10^{-2}$ C mm^{-2} electron dose. This aspect can be attributed to the fact that in this specific case the benefit of the surface roughening on the SEY reduction excels the deteriorative consequences on SEY caused by the compositional surface changes including the transformation from hydroxide to a particular oxide phase at cryogenic temperature.[6] The results demonstrate that it is possible to optimize the laser treatment to obtain a surface with an SEY value of 1.5 before conditioning, which reduces

the risk of detachment of particulates and achieves electron cloud suppression after conditioning.

4.5 Laser-treated beam screen segment – surface resistance

A comparison of the surface resistance of a standard LHC beam screen with pure copper surface and that of the processed BS shown in Fig. 4, which underwent the selective $4 \times 20°$ laser treatment, was performed using the shielded pair method.[46,47] The result is that the surface resistance of the laser-treated regions with longitudinal trenches of 15–19 μm depth is 1.3–1.6 times higher than that of the untreated copper at 4.2 K within the investigated frequency range. These findings are consistent with previous studies.[29] Considering the locally higher surface resistance in the four treated segments at the BS corners, the possible impact on the real part of the LHC beam screen longitudinal beam impedance can be determined by further analysis. Fig. 10 presents the results of the computer simulation technology (CST) Wakefield Solver analysis on the increase of the real part of the longitudinal beam impedance as a function of frequency. The figure compares a standard LHC beam screen with the selectively laser-treated beam screen indicating that an increase of up to only 3% can be expected. The main reason for this negligible increment in the beam screen impedance lies within the location of the laser processing at the 4 corners, where the lowest image current density is induced by the circulating beam during operation. The left plot in Fig. 11 shows the normalized magnitude of the magnetic field strength generated by the particle beam, as a density map. The magnitude of magnetic field vector strength in-plane with the BS surface is proportional to the locally induced image current. Fig. 11 includes on its right side the angular dependence of these quantities with an indication of the laser-treated regions in gray. The maximum current is induced in the upper and lower flat regions of the beam screen, which are closest to the beam. The positions of
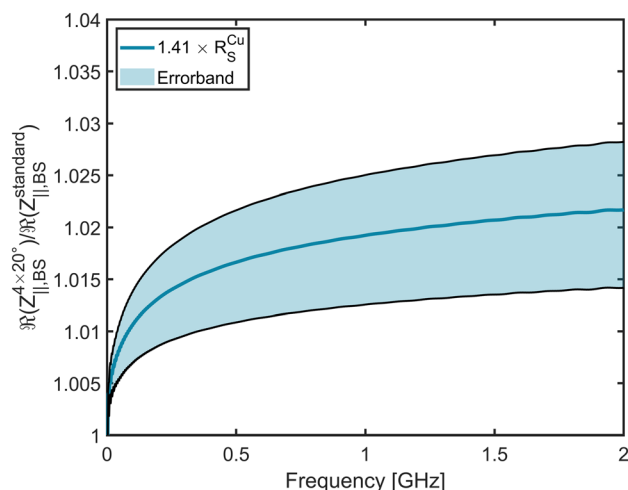

Fig. 10 Comparison of real part of the longitudinal beam impedance: ratio between selective laser treated LHC beam screen and standard LHC beam screen including error bands.
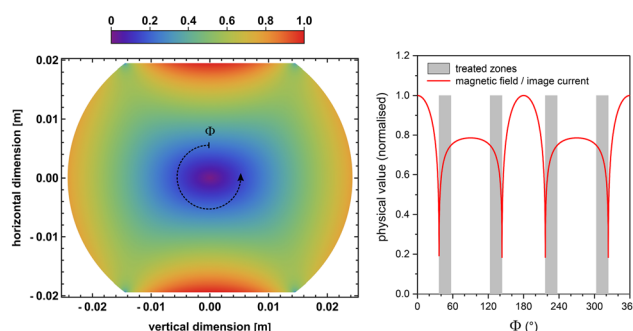

Fig. 11 Left: Density plot of the normalized magnetic field strength distribution inside the LHC beam screens generated by the circulating particle beam. Right: Angular azimuthal dependence of the normalized magnetic field strength at the beam screen surface and the resulting image current with $\Phi = 0°$ defined at the closest vertical point to the center of the beam screen. The laser treated regions are highlighted in gray.

the laser treatment correspond with the lowest magnitudes in induced surface current density.

5 Conclusions

A selective laser treatment process was developed that allows to suppress EC formation in quadrupole magnet assemblies of the LHC to improve the beam quality. Thereby the ultrashort pulse laser beam is scanned in parallel longitudinal lines across the inner beam screen surface. Electron cloud simulations and material characterizations showed that a laser treatment in the high-intensity electron cloud areas with an initial SEY maximum of 1.5 is sufficient to suppress electron clouds after conditioning *via* beam scrubbing, particularly in the center of the beam screen. The selective laser treatment of a beam screen segment of 40 cm in length demonstrated the applicability of the method. The SEY of the roughened surfaces was in the range of δ_{max} 1.28–1.52, which decreased under electron irradiation to 1.0 at room temperature and cryogenic temperature. The ablation depth was found to be between 15 and 19 μm, which is below the upper acceptance limit. The variation in SEY and ablation depth could be minimized in the future by the use of a diffractive optical element (DOE) that enlarges the focal depth and makes the treatment less sensitive to under-/over-focusing.[58] Based on centrifugation tests, it is concluded that particulate detachment is not crucial for surfaces with $\delta_{max} > 1$ at a force density of 3 N mm^{-3}. Finally, impedance measurements showed that a selective treatment with longitudinally aligned trenches does not increase the longitudinal beam impedance significantly compared to a smooth copper beam screen surface. The presented laser treatment could be applied during the long shutdown 3 of the LHC to selected Q5 standalone magnets located next to the interaction points 1 (ATLAS detector) and 5 (CMS detector). The proposed scenario of the 4 × 20° pattern is tailored to mitigate negative effects of the EC on beam quality in quadrupole magnets. In this case the remaining side electron bands do not interfere with passing particles. One could clearly extend the treated regions to suppress these side effects further with the consequences of extended processing time and enhanced material ablation.

Data availability

For our manuscript "Selective laser processing of particle accelerator beam screen surfaces for electron cloud mitigation", the data is available within the article and its ESI† (ASCII data).

Author contributions

Elena Bez: conceptualization (equal); formal analysis (equal); investigation (equal); methodology (equal); visualization (equal); writing – original draft (equal); writing – review & editing (equal). Ana Karen Reascos Portilla: formal analysis (equal); investigation (equal); methodology (equal); writing – review & editing (supporting). Valentine Petit: formal analysis (equal); investigation (equal); methodology (equal); visualization (equal); writing – review & editing (equal). Konstantinos Paraschou: conceptualization (equal); formal analysis (equal); investigation (equal); methodology (equal); visualization (equal); writing – original draft (equal); writing – review & editing (equal). Lotta Mether: conceptualization (supporting); formal analysis (equal); investigation (equal); methodology (supporting); writing – review & editing (equal). Kristóf Brunner: conceptualization (equal); formal analysis (supporting); investigation (equal); methodology (equal); writing – review & editing (equal). Patrick Krkotić: conceptualization (equal); formal analysis (equal); investigation (equal); methodology (equal); visualization (equal); writing – original draft (equal); writing – review v editing (equal). Yasemin Askar: formal analysis (equal; investigation (equal); methodology (equal); writing – original draft (supporting); writing – review & editing (equal). Sergio Calatroni: conceptualization (equal); investigation (supporting); methodology (equal); project administration (equal); validation (equal); writing – review & editing (equal). Mauro Taborelli: conceptualization (equal); investigation (supporting); methodology (supporting); project administration (equal); validation (equal); writing – review & editing (equal). Marcel Himmerlich: conceptualization (equal); formal analysis (equal); investigation (equal); methodology (equal); project administration (equal); supervision (lead); validation (equal); writing – original draft (equal); writing – review & editing (equal).

Conflicts of interest

The authors declare that they have no conflict of interest.

Acknowledgements

References

1 L. Evans and P. Bryant, *J. Instrum.*, 2008, **3**, S08001.

2 O. Aberle, *et al.*, High-Luminosity Large Hadron Collider (HL-LHC): Technical design report, *CERN Yellow Reports: Monographs*, 2020, **https://cds.cern.ch/record/2749422**.

© 2025 The Author(s). Published by the Royal Society of Chemistry

RSC Appl. Interfaces, 2025, **2**, 521–533 | 531

3 G. Arduini, J. Barranco, A. Bertarelli, N. Biancacci, R. Bruce, O. Brüning, X. Buffat, Y. Cai, L. Carver, S. Fartoukh, M. Giovannozzi, G. Iadarola, K. Li, A. Lechner, L. M. Medrano, E. Métral, Y. Nosochkov, Y. Papaphilippou, D. Pellegrini, T. Pieloni, J. Qiang, S. Redaelli, A. Romano, L. Rossi, G. Rumolo, B. Salvant, M. Schenk, C. Tambasco, R. Tomás, S. Valishev and F. V. der Veken, *J. Instrum.*, 2016, **11**, C12081.

4 N. Mounet, R. Tomás, D. Amorim, C. Antuono, N. Biancacci, H. Bartosik, P. Baudrenghien, R. Bruce, X. Buffat, R. Calaga, R. D. Maria, C. Droin, L. Giacomel, M. Giovannozzi, G. Iadarola, S. Kostoglou, A. Kurtulus, B. Lindström, L. Mether, E. Métral, Y. Papaphilippou, K. Paraschou, S. Redaelli, G. Rumolo, B. Salvant, L. Sito, G. Sterbini and C. Zannini, *J. Instrum.*, 2024, **19**, T05016.

5 V. Petit, M. Taborelli, H. Neupert, P. Chiggiato and M. Belhaj, *Phys. Rev. Accel. Beams*, 2019, **22**, 083101.

6 V. Petit, M. Taborelli, D. A. Zanin, M. Himmerlich, H. Neupert, P. Chiggiato and G. Iadarola, *Commun. Phys.*, 2021, **4**, 192.

7 C. Yin Vallgren, G. Arduini, J. Bauche, S. Calatroni, P. Chiggiato, K. Cornelis, P. C. Pinto, B. Henrist, E. Métral, H. Neupert, G. Rumolo, E. Shaposhnikova and M. Taborelli, *Phys. Rev. Spec. Top.–Accel. Beams*, 2011, **14**, 071001.

8 P. Costa Pinto, S. Calatroni, H. Neupert, D. Letant-Delrieux, P. Edwards, P. Chiggiato, M. Taborelli, W. Vollenberg, C. Yin-Vallgren, J. Colaux and S. Lucas, *Vacuum*, 2013, **98**, 29–36.

9 H. Moreno Fernández, M. Himmerlich, P. Costa Pinto, J. Coroa, D. Sousa, A. Baris and M. Taborelli, *Appl. Surf. Sci.*, 2021, **542**, 148552.

10 G. Skripka and G. Iadarola, Beam-induced heat loads on the beam screens of the HL-LHC arcs, *CERN Technical report: CERN-ACC-NOTE-2019-0041*, 2019, **https://cds.cern.ch/record/2692753**.

11 W. Vollenberg, P. Chiggiato, P. Costa Pinto, P. Cruikshank, H. Moreno, C. Pasquino, J. Perez Espinos and M. Taborelli, Amorphous carbon coating in SPS, *Proc. 12th Int. Particle Accelerator Conf. (IPAC 2021)*, 2021, **https://accelconf.web.cern.ch/ipac2021/doi/JACoW-IPAC2021-WEPAB338.html**.

12 A. R. Granadeiro Costa, S. Fiotakis and P. Costa Pinto, In-situ amorphous carbon (a-C) coating of Q5L8 standalone magnet, *CERN EDMS report*, 2020, **https://edms.cern.ch/document/2441196/1**.

13 The ALICE Collaboration, *J. Instrum.*, 2008, **3**, S08002.

14 The LHCb Collaboration, *J. Instrum.*, 2008, **3**, S08005.

15 The CMS Collaboration, *J. Instrum.*, 2008, **3**, S08004.

16 The ATLAS Collaboration, *J. Instrum.*, 2008, **3**, S08003.

17 R. Valizadeh, O. B. Malyshev, S. Wang, S. A. Zolotovskaya, W. Allan Gillespie and A. Abdolvand, *Appl. Phys. Lett.*, 2014, **105**, 231605.

18 S. Calatroni, E. Garcia-Tabares Valdivieso, H. Neupert, V. Nistor, A. T. Perez Fontenla, M. Taborelli, P. Chiggiato, O. Malyshev, R. Valizadeh, S. Wackerow, S. A. Zolotovskaya, W. A. Gillespie and A. Abdolvand, *Phys. Rev. Accel. Beams*, 2017, **20**, 113201.

19 D. Bajek, S. Wackerow, D. A. Zanin, L. Baudin, K. Bogdanowicz, E. G.-T. Valdivieso, S. Calatroni, B. Di

Girolamo, M. Sitko, M. Himmerlich, M. Taborelli, P. Chiggiato and A. Abdolvand, *Sci. Rep.*, 2020, **10**, 250.

20 P. Lorenz, M. Himmerlich, M. Ehrhardt, E. Bez, K. Bogdanowicz, M. Taborelli and K. Zimmer, *Lasers Manuf. Mater. Process.*, 2022, **9**, 135–150.

21 P. Lorenz, E. Bez, M. Himmerlich, M. Ehrhardt, M. Taborelli and K. Zimmer, *Procedia CIRP*, 2022, **111**, 662–666.

22 P. Lorenz, E. Bez, M. Himmerlich, M. Ehrhardt, M. Taborelli and K. Zimmer, *J. Micro Nano-Manuf.*, 2023, **18**, 121–126.

23 E. Bez, M. Himmerlich, P. Lorenz, M. Ehrhardt, A. G. Gunn, S. Pfeiffer, M. Rimoldi, M. Taborelli, K. Zimmer, P. Chiggiato and A. Anders, *J. Appl. Phys.*, 2023, **133**, 035303.

24 O. Domínguez, K. Li, G. Arduini, E. Métral, G. Rumolo, F. Zimmermann and H. M. Cuna, *Phys. Rev. Spec. Top.–Accel. Beams*, 2013, **16**, 011003.

25 G. Iadarola, B. Bradu, L. Mether, K. Paraschou, V. Petit, G. Rumolo, L. Sabato, G. Skripka, M. Taborelli and L. Tavian, Progress in Mastering Electron Clouds at the Large Hadron Collider, *Proc. 12th Int. Particle Accelerator Conf. IPAC2021*, 2021, **https://jacow.org/ipac2021/papers/tuxa03.pdf**.

26 G. Arduini, V. Baglin, H. Bartosik, L. Bottura, C. Bracco, B. Bradu, G. Bregliozzi, K. Brodzinski, R. Bruce, M. Calviani, P. Chiggiato, P. Cruikshank, S. Claudet, D. Delikaris, S. Fartoukh, C. Garion, M. Himmerlich, M. Hostettler, G. Iadarola, S. Kostoglou, S. L. Naour, A. Lechner, T. Lefevre, L. Mether, Y. Papaphilippou, V. Petit, M. Pojer, A. Poyet, S. Redaelli, F. R. Mateos, G. Rumolo, B. Salvant, F. S. Galan, A. Siemko, M. Solfaroli-Camillocci, G. Sterbini, M. Taborelli, L. Tavian, H. Timko, J.-P. Tock, A. Verweij, M. Wendt, J. Wenninger, D. Wollmann and C. Y. Vallgren, *J. Instrum.*, 2024, **19**, P05061.

27 V. Baglin, *Vacuum*, 2017, **138**, 112–119.

28 E. Bez, M. Himmerlich, B. Beaudou, A. K. Reascos Portilla, S. Wackerow, M. Rimoldi, S. Pfeiffer, M. Wiesendanger, F. Benabid, M. Taborelli, A. Abdolvand and P. Chiggiato, *Rev. Sci. Instrum.*, 2023, **94**, 103007.

29 S. Calatroni, M. Arzeo, S. Aull, M. Himmerlich, P. Costa Pinto, W. Vollenberg, B. Di Girolamo, P. Cruikshank, P. Chiggiato, D. Bajek, S. Wackerow and A. Abdolvand, *Phys. Rev. Accel. Beams*, 2019, **22**, 063101.

30 P. Krkotić, S. Calatroni, M. Himmerlich, H. Neupert, A. T. Perez-Fontenla, S. Wackerow and A. Abdolvand, *J. Phys.: Conf. Ser.*, 2024, **2687**, 082029.

31 A. Lechner, P. Bélanger, I. Efthymiopoulos, L. Grob, B. Lindstrom, R. Schmidt and D. Wollmann, *Phys. Rev. Accel. Beams*, 2022, **25**, 041001.

32 P. Dijkstal, G. Iadarola, L. Mether and G. Rumolo, Simulation studies on the electron cloud build-up in the elements of the LHC Arcs at 6.5 TeV, *CERN Technical report: CERN-ACC-NOTE-2017-0057*, 2017, **https://cds.cern.ch/record/2289940**.

33 G. Skripka, G. Iadarola, L. Mether and G. Rumolo, *Eur. Phys. J. Plus*, 2022, **137**, 849.

34 G. Iadarola, Electron cloud studies for CERN particle accelerators and simulation code development, *PhD thesis*,

Università degli Studi di Napoli Federico II, Napoli, Italy, 2014, https://cds.cern.ch/record/1705520.

35 R. Cimino, M. Commisso, D. R. Grosso, T. Demma, V. Baglin, R. Flammini and R. Larciprete, *Phys. Rev. Lett.*, 2012, **109**, 064801.

36 G. Iadarola, E. Belli, K. Li, L. Mether, A. Romano and G. Rumolo, Evolution of Python Tools for the Simulation of Electron Cloud Effects, *Proc. 8th Int. Particle Accelerator Conf. (IPAC 2017)*, 2017, https://cds.cern.ch/record/2289165.

37 G. Iadarola, Modelling the interaction of a relativistic beam particle with an electron cloud, *CERN Technical report: CERN-ACC-NOTE-2019-0033*, 2019, https://cds.cern.ch/record/2684858.

38 E. Wulff and G. Iadarola, Implementation and benchmarking of the Furman-Pivi model for Secondary Electron Emission in the PyECLOUD simulation code, *CERN Technical report: CERN-ACC-NOTE-2019-0029*, 2019, https://cds.cern.ch/record/2683285.

39 A. Romano, O. Boine-Frankenheim, X. Buffat, G. Iadarola and G. Rumolo, *Phys. Rev. Accel. Beams*, 2018, **21**, 061002.

40 L. Sabato, G. Iadarola and L. Mether, Numerical simulations studies on single-bunch instabilities driven by electron clouds at the LHC, *CERN Technical report: CERN-ACC-NOTE-2020-0050*, 2020, https://cds.cern.ch/record/2733028.

41 K. Paraschou, Studies of incoherent effects for the upgrade of the large hardon collider and detector applications, *PhD thesis*, Aristotle University of Thessaloniki, Greece, 2023, DOI: 10.26262/heal.auth.ir.348933.

42 V. Petit, Conditioning of surfaces in particle accelerators, *PhD thesis*, Université Toulouse, France, 2020, https://hal.science/tel-02919120/file/DPHY20102.1597843660-4.pdf.

43 S. Marinoni, An ultra-high vacuum system for secondary electron yield measurements and electron-conditioning of particle accelerators materials at cryogenic temperatures: commissioning and first experiments, *M.Sc. thesis*, Politecnico di Milano, Italy, 2022, https://cds.cern.ch/record/2891850.

44 E. Stranelova, Characterisation and modification of copper surfaces for cryogenic vacuum components of particle accelerators, *M.Sc. thesis*, University of Chemistry and Technology, Prague, Czech Republic, 2023, https://cds.cern.ch/record/2891854.

45 L. Baudin, Laser treated surfaces in particle accelerators: relation between superficial topography, particle adhesion

and compatibility for ultra-high vacuum applications, *PhD thesis*, Université Paris Sciences et Lettres, France, 2020, http://www.theses.fr/2020UPSLM052.

46 K. Brunner, D. Barna, S. Calatroni and F. Caspers, Shielded Pair Method for Cylindrical Surface Resistance Measurement at Cryogenic Temperature, 2021, *Proc. 12th Int. Particle Accelerator Conf. (IPAC 2021)*, DOI: 10.18429/JACoW-IPAC2021-MOPAB364.

47 K. Brunner, P. Krkotić, S. Calatroni and D. Barna, *Instruments*, 2024, **8**, 43.

48 R. Cimino, I. R. Collins, M. A. Furman, M. Pivi, F. Ruggiero, G. Rumolo and F. Zimmermann, *Phys. Rev. Lett.*, 2004, **93**, 014801.

49 N. Mahne, V. Baglin, I. Collins, A. Giglia, L. Pasquali, M. Pedio, S. Nannarone and R. Cimino, *Appl. Surf. Sci.*, 2004, **235**, 221–226.

50 G. Guillermo, D. Sagan and F. Zimmermann, *Phys. Rev. Accel. Beams*, 2018, **21**, 021001.

51 J. Bonse and S. Gräf, *Laser Photonics Rev.*, 2020, **14**, 2000215.

52 J. Nivas, M. Valadan, M. Salvatore, R. Fittipaldi, M. Himmerlich, M. Rimoldi, A. Passarelli, E. Allahyari, S. Oscurato, A. Vecchione, C. Altucci, S. Amoruso, A. Andreone, S. Calatroni and M. Masullo, *Surf. Interfaces*, 2021, **25**, 101179.

53 M. Himmerlich, D. A. Zanin, M. Taborelli, A. R. Granadeiro Costa, P. Costa Pinto, L. Lain Amador, W. Vollenberg, A. Baris, E. Garcia-Tabares Valdivieso, A. T. Perez Fontenla, S. Wackerow and A. Abdolvand, *Adv. Mater. Interfaces*, 2023, **10**, 2201671.

54 E. Bez, Laser-induced surface structuring for electron cloud mitigation in particle accelerators, *PhD thesis*, Universität Leipzig, Germany, 2024, https://nbn-resolving.org/urn:nbn:de:bsz:15-qucosa2-948112.

55 M. C. Biesinger, *Surf. Interface Anal.*, 2017, **49**, 1325–1334.

56 J. J. J. Nivas, M. Hu, M. Valadan, M. Salvatore, R. Fittipaldi, M. Himmerlich, E. Bez, M. Rimoldi, A. Passarelli, S. L. Oscurato, A. Vecchione, C. Altucci, S. Amoruso, A. Andreone, S. Calatroni and M. Rosaria Masullo, *Appl. Surf. Sci.*, 2023, 156908.

57 V. Petit, P. Chiggiato, M. Himmerlich, S. Marinoni, H. Neupert, M. Taborelli and L. Tavian, *J. Phys.: Conf. Ser.*, 2023, **2420**, 012088.

58 R. Uren, A. Din, S. Wackerow, E. Bez, S. Pfeiffer, M. Rimoldi, M. Himmerlich, M. Taborelli and A. Abdolvand, *Opt. Mater. Express*, 2023, **13**, 1228–1240.